Proc. of the International Conference on Electrical, Computer and Energy Technologies (ICECET)
9-10 December 2021, Cape Town-South Africa

Joint Optimization of Electric Vehicle Fast Charging and DC Fast Charging Station

Mohammad Hossein Abbasi
Department of Automotive Engineering
Clemson University
Greenville, SC, USA
mabbasi@clemson.edu

Jiangfeng Zhang
Department of Automotive Engineering
Clemson University
Greenville, SC, USA
jiangfz@clemson.edu

2021 International Conference on Electrical, Computer and Energy Technologies (ICECET) | 978-1-6654-4231-2/21/$31.00 ©2021 IEEE | DOI: 10.1109/ICECET52533.2021.9698541

***Abstract*—Joint optimization of electric vehicle (EV) fast charging and DC fast charging (DCFC) station problems is presented in this paper. An electro-thermal-aging model is used for modeling EV's battery cell. The model is then expanded from a single cell to a battery pack based on the structure of commercially available EV batteries in the market. Moreover, the limitations imposed by the DCFC station are properly considered in the problem's constraints, including restrictions due to the cost of electricity, especially demand charge, and port power rating of chargers. The station's profit is maximized, and its cost is minimized considering demand charge and energy charge tariffs. Finally, the problem is discretized and numerically evaluated in a detailed case study.**

***Index Terms*—electric vehicles, fast charging, DC fast charging station, electro-thermal-aging battery model, battery pack model, energy and demand charge**

NOMENCLATURE

t	Time
n	Number of ports at the station
$z(t)$	State of charge (SOC)
$I(t)$	Charging current
$V_t(t)$	Terminal voltage
$V_1(t)$	First RC pair Voltage
$V_2(t)$	Second RC pair Voltage
$T_c(t)$	Core temperature
$T_s(t)$	Surface temperature
$SOH(t)$	State of health
$P(n,t)$	Output power of port n
$P^{\max}_{\text{station}}$	Station power cap
$P^{\max}_{\text{charger}}$	Port power rating
α	Weighting parameter
C_b	Battery capacity
R_0	Equivalent series resistance
R_1	First RC pair resistance
R_2	Second RC pair resistance
C_1	First RC pair capacitance
C_2	Second RC pair capacitance
R_c	Heat conduction resistance
R_u	Convection resistance
R_m	Cell-to-cell heat transfer resistance
C_c	Core heat capacity
C_s	Surface heat capacity
T_f	Ambient temperature
OCV	Open circuit voltage
$z_{\min}$	Minimum of state of charge
$z_{\max}$	Maximum of state of charge
$I_{\min}$	Minimum current
$I_{\max}$	Maximum current
$V_{t,\min}$	Minimum terminal voltage
$V_{t,\max}$	Maximum terminal voltage
$T_{c,\min}$	Minimum core temperature
$T_{c,\max}$	Maximum core temperature
ΔQ	Capacity loss percentage
c	C-rate
B	Pre-exponential factor
E_a	Activation energy
R	Gas constant
A_h	Ampere hour throughput
γ	Power law factor
λ_b	Energy charge rate
λ_s	Station's selling price
λ_d	Demand charge rate
$P_d^{\max}$	Station's maximum power

I. INTRODUCTION

Lithium-ion batteries are mainly used in electric vehicles (EVs), consumer electronics, and electricity network storage facilities. In particular, utilizing Li-ion batteries as an energy source in the automotive industry puts EVs into competition with gasoline vehicles. Refueling gasoline vehicles is faster than recharging EV batteries which gives rise to the challenge of finding approaches to charge batteries faster. The challenge stems from the exacerbating nature of fast charging that degrades the battery and reduces its capacity, while slow charging increases customer's range anxiety. The consensus on the definition of fast charging is to add 200 miles of driving range within 10 minutes of charge [1]. Accordingly, care must be taken into consideration when trading off between fast charging and battery degradation [2].

Three distinct manners have been adopted in the literature to tackle the fast charging problem. In the traditional approach, which is primarily based on constant-current constant-voltage (CCCV) charging [3], heuristic protocols are investigated to reduce the charging time [4]. The conventional approaches lack control over temperature and degradation [5], and do not guarantee optimality [6]. The second category enjoys empirical models [7] that are fast and easy to implement [5] but do not encompass internal battery states [8]. The third strategy exploits electrochemical models [9] that are accurate at the cost of complexity, and the measurement of their parameters is not straightforward. To circumvent interactability, these models are always simplified in practice. In addition, thermal and aging models can be coupled with the empirical or physics-based models. Nevertheless, most literature focuses on modeling a cell, while EVs integrate thousands of cells in their battery packs. The combination of cells in a pack could exhibit emergent behaviors that are not captured by the cell model [10]. Further, packing the cells elevates the implications of nonlinear aging characteristics of the battery [11].

A key role of DC fast charging (DCFC) stations is to cope with range anxiety [12]. DCFC stations induce stability, resilience, and efficiency problems for the power grid [13]. To address the issues, energy storage systems [14], and renewable energy generation [15] are proposed. However, storage systems are associated with infrastructure costs, and renewable generation effectively mitigates the costs only when the demand is high. The studies that deal with fast charging stations are mainly concerned with the quality of service or minimizing the costs. Thus, the mutual effect of the EV fast-charging problem and the station's optimization problem is not properly analyzed. Previous studies do not include the details of EV fast charging in the station problem or vice versa. Additionally, the battery pack model is rarely considered in the literature.

The present work combines the optimization problems of DCFC station and EV fast charging. The goal is to find an optimal point where the EVs are charged as fast as possible, and the station's profit is maximized. The novelty of our work is that we combine the EV fast charging and the station profit maximization problems to include their impact on each other. We firstly extend the cell model to the pack model, then incorporate pack level thermal and aging models, and finally solve the fast charging problem jointly with the station problem.

II. Proposed Methodology

In this section, the optimization problem of EV fast charging and DC fast charging station is formulated. In the following, the formulation of the four categories of constraints is presented, followed by the formulation of the overall problem.

A. Equivalent Circuit Model (ECM)

Firstly, the equivalent circuit model of a cell is modeled using a second-order ECM. The model emulates the voltage behavior of lithium iron phosphate ($LiFePO_4$/graphite) cell (A123 ANR26650M1). The independent variables of the model are state of charge (SOC), $z(t)$, and charging/discharging current, $I(t)$. Secondly, the model is modified to represent the behavior of a battery pack rather than a single cell. To this end, a battery pack based on Tesla's 85 kWh pack is considered. We assume that the pack consists of ANR26650M1 cells. Tesla's 85 kWh pack comprises 16 modules connected in series. Each module contains six groups of 74 cells that are wired in parallel. The six groups in each module are connected in series. All in all, the pack consists of 7104 cells ($16 \times 6 \times 74$).

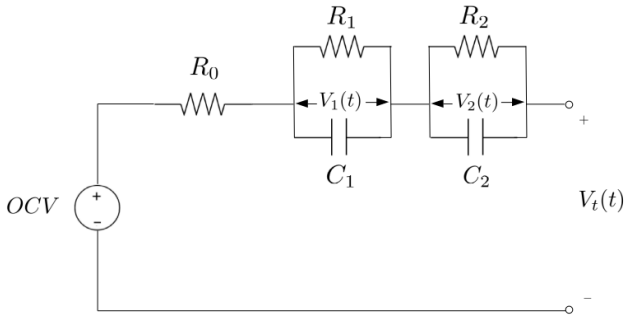

Fig. 1. Second-order equivalent circuit model

The ECM is depicted in Fig. 1. It consists of an open circuit voltage, OCV, an equivalent series resistance, R_0, and two pairs of resistor-capacitors. The governing differential equations are as follows:

$$\frac{dz(t)}{dt} = \frac{I(t)}{C_b}, \tag{1}$$

$$\frac{dV_1(t)}{dt} = -\frac{V_1(t)}{R_1 C_1} + \frac{I(t)}{C_1}, \tag{2}$$

$$\frac{dV_2(t)}{dt} = -\frac{V_2(t)}{R_2 C_2} + \frac{I(t)}{C_2}, \tag{3}$$

$$V_t(t) = OCV + V_1(t) + V_2(t) + R_0 I(t), \tag{4}$$

where $z(t)$ is the state of charge expressed in percentage, C_b is the battery's nominal capacity in Ah, $I(t)$ is the current in ampere and is considered negative for discharge. Equation (1) expresses the relationship between the current and SOC. Based on (1), when the current is positive, the SOC will increase and vice versa. Therefore, a positive current means the battery is charging. Equations (2), (3) respectively yield the value of the two voltages across the first and the second RC pairs. Finally, equation (4) represents terminal voltage, $V_t(t)$. Note that if the current is positive, $V_1(t)$ and $V_2(t)$ are also positive. Accordingly, the terminal voltage is greater than open-circuit voltage, OCV, meaning that the battery is charging. Conversely, during discharge, the terminal voltage is less than OCV.

Next, the second-order ECM model is generalized to denote the battery pack instead of a single cell.

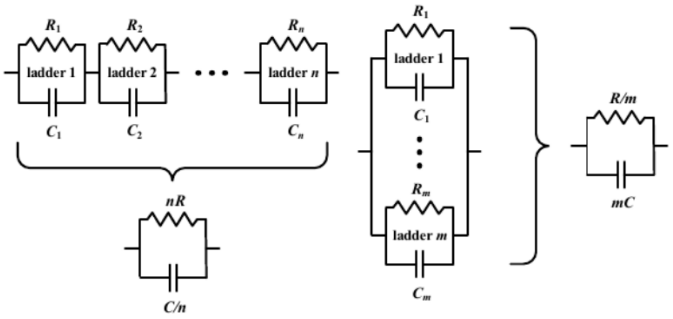

Fig. 2. Replacing n identical series connected RC pairs and m similar parallel wired RC pairs with equivalent pairs (adopted from [16]).

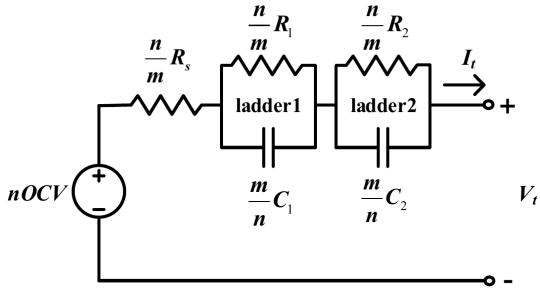

Fig. 3. Second-order ECM for the battery pack (adopted from [16]).

B. Battery Pack Model

The structure of the pack consists of 16 modules, with six groups in each module, where each group contains 74 cells. The 74 cells are connected in parallel, while groups and modules are wired in series. Consequently, we can assume that the pack structure is as follows: There are 74 groups of cells connected in parallel. Each group comprises 96 (16×6) cells that are connected in series. In other words, the structure looks like a matrix with 74 rows and 96 columns.

Each cell is modeled via a second-order equivalent circuit model. With the assumption that the cells are identical, we will find a second-order equivalent circuit model for the battery pack. In this regard, using Kirchhoff's laws, every two identical RC pairs that are connected in series can be substituted with an R_eC_e pair in which equivalent resistance is equal to the summation of the two identical resistances, i.e., $R_e = 2R$. The equivalent capacitance is equal to the half capacitance of each of the identical capacitors, i.e., $C_e = C/2$. Therefore, as shown in Fig. 2, n identical RC pairs wired in series can be supplanted by an R_eC_e pair with $R_e = nR$ and $C_e = C/n$. Finally, in our battery pack, wherein 96 cells are connected in series, all the R_1C_1 and R_2C_2 pairs can be replaced by

$$R_{1,new} = 96R_1, \tag{5}$$

$$C_{1,new} = \frac{1}{96}C_1, \tag{6}$$

and

$$R_{2,new} = 96R_2, \tag{7}$$

$$C_{2,new} = \frac{1}{96}C_2, \tag{8}$$

respectively.

In a similar fashion, m identical RC pairs that are connected in parallel can be replaced with an R_eC_e pair where $R_e = R/m$ and $C_e = mC$ (see Fig. 2). Since the series-connected parts are already replaced with equivalent RC pairs, the remaining part consists of 74 new RC pairs connected in parallel. Thus, as illustrated in Fig. 3, we can write:

$$R_{1,\text{pack}} = \frac{96}{74}R_1, \tag{9}$$

$$C_{1,\text{pack}} = \frac{74}{96}C_1, \tag{10}$$

and

$$R_{2,\text{pack}} = \frac{96}{74}R_2, \tag{11}$$

$$C_{2,\text{pack}} = \frac{74}{96}C_2. \tag{12}$$

The reason that OCV is only multiplied by 96 is that the voltage across parallel connections remains the same, while it is equal to the summation of the voltages of series-connected elements. It is worth noting that the parallel connections increase the pack's maximum current rate and, in turn, boost the battery capacity. Hence, the pack's C-rate is multiplied by 74.

The following section presents a two-state thermal model to capture the behavior of the battery's core and surface temperatures.

C. Thermal Model

By considering the surface and core temperatures of the cell, the ruling equations are as follows:

$$\frac{dT_c(t)}{dt} = \frac{T_s(t) - T_c(t)}{R_cC_c} + \frac{I(t)(OCV(z) - V_t)}{C_c}, \tag{13}$$

$$\frac{dT_s(t)}{dt} = \frac{T_f(t) - T_s(t)}{R_uC_s} - \frac{T_s(t) - T_c(t)}{R_cC_s}, \tag{14}$$

where T_f, $T_c(t)$ and $T_s(t)$ are ambient, core and surface temperatures, respectively. Convection resistance, R_u, models convective cooling that occurs via the surface of the cell. On the other hand, conduction resistance, R_c, indicates the resistance against the heat transfer between the surface and the core of the cylindrical cell. The heat capacities of the core and the surface, C_c and C_s, alter the incidence of temperature change.

In order to modify the cell's thermal model and find an appropriate model for the battery pack, it suffices to factor in the heat exchange between adjacent cells in the pack [17]. As a result, (14) is rewritten as follows:

$$\frac{dT_{s_k}(t)}{dt} = \frac{T_f(t) - T_{s_k}(t)}{R_uC_s} - \frac{T_{s_k}(t) - T_c(t)}{R_cC_s} + \frac{T_{s_k} - T_{s_{k+1}}}{R_mC_s} + \frac{T_{s_k} - T_{s_{k-1}}}{R_mC_s}. \tag{15}$$

The parameters of the electro-thermal model are adopted from [18] where the model is validated over the SOC range

of 25% to 100%, temperature range of 5°C to 38°C, and the maximum current of 22C.

The following section deals with the battery aging model.

D. Battery Aging Model

The model is obtained from [19] and established using a cycle-test matrix. The experiment is conducted on $LiFePO_4$/graphite cells. The tests are performed over different ranges of C-rates, from C/2 to 10C, temperatures, from -30°C to 60°C, and state of charge levels, between 10% and 90%. The results showed that the capacity drop mostly depends on time and temperature at the low C-rates, while charge/discharge rate becomes essential at the high C-rates. A power law equation is exploited to constitute the life model, in which an Arrhenius correlation that represents temperature effect and charge throughput formulate capacity fade. The empirical model is as follows:

$$\Delta Q = B \exp\left(-\frac{E_a}{RT_c}\right) A_h^{\gamma}, \tag{16}$$

where ΔQ denotes capacity loss percentage, and E_a indicates activation energy (J/mol). The ampere-hour throughput, A_h, is calculated as:

$$A_h = (\text{cycle \#}) \times (\text{depth of discharge}) \times (\text{cell capacity}). \tag{17}$$

In [19], high C-rates are defined as the charging/discharging currents over C/2. In this respect, the activation energy is estimated for high C-rates as follows:

$$E_a = 31700 - 370.3 \times c. \tag{18}$$

Based on [20], the end of life of an electric vehicle battery is when 20% of the capacity is lost. Therefore, the ampere-hour throughput corresponding to $\Delta Q = 20\%$ is as the following:

$$A_{h,20\%} = \left[\frac{20}{B \exp\left(-\frac{E_a}{RT_c}\right)}\right]^{\frac{1}{\gamma}}. \tag{19}$$

Accordingly, the required number of cycles until $A_{h,20\%}$ is computed as follows:

$$N = \frac{3600\ A_{h,20\%}}{C_b}, \tag{20}$$

where the coefficient 3600 is utilized to change ampere-hour into ampere-second.

The next step is to use N to formulate the state of health (SOH). The SOH should reduce from 100% to zero percent when 20% of the battery pack's capacity is dropped. The following formula models SOH:

$$SOH(t) = SOH(t_0) - \frac{\int_{t_0}^{t} |I(\tau)| d\tau}{2NC_b}, \tag{21}$$

where t_0 is starting time. Based on (21), SOH is 100% at the beginning of the battery's life and is zero when 20% of the lithium inventory is lost.

Lastly, the integral form of SOH is converted to point form by derivating (21) as the following:

$$\frac{dSOH(t)}{dt} = -\frac{|I(t)|}{2NC_b}. \tag{22}$$

The formula of SOH derivative is similar to the rate of change in SOH, i.e., equation (1). It merits mentioning that (16) incorporates both cycle life and calendar aging.

The following section addresses the formulation of the DC fast charging station's profit maximization problem.

E. DC Fast Charging Station Optimization Model

Now we turn to formulating the optimization problem of the DCFC station. The problem is a linear optimization problem in which the profit of selling energy to EVs is maximized, and the cost of purchasing electricity from the grid is minimized. It is assumed that the DCFC station procures electricity directly from the network, and it does not own storage facilities or PV pannels. Furthermore, the electricity prices are based on an electricity tariff, including energy charge and demand charge [12].

The power rating of the chargers range from 50kW to 450kW [21], including 50kW, 120kW, 150kW, 250kW, 350kW, and 450kW charging posts. In this study, a 250kW charger is selected.

The proposed optimization problem for the DC fast charging station is as follows:

$$\min \quad \sum_n \sum_t P(n,t)(\lambda_b - \lambda_s) + P_d^{\max} \lambda_d, \tag{23}$$

subject to

$$\sum_n P(n,t) \le P_{\text{station}}^{\max}, \tag{24}$$

$$P(n,t) \le P_{\text{charger}}^{\max}, \tag{25}$$

$$P_{\text{station}}^{\max} = n \cdot P_{\text{charger}}^{\max}, \tag{26}$$

$$P(n,t) = I(t).V_t(t), \tag{27}$$

$$P_d^{\max} = \max\left\{\sum_n P(n,t)\right\}, \tag{28}$$

where n indicates the number of ports in the station. Equation (23) is the objective in which the first part states that the total profit of selling power over all ports and in all time slots is deducted from the cost of purchasing that amount of energy. The second part denotes the demand charge that is equal to the maximum power drawn from the grid by the station multiplied by the demand charge rate. Equation (24) states that the station's power limitation caps the summation of the power of all ports. The power rating restriction of the chargers is expressed via constraint (25), followed by (26) that establishes the relationship between power ratings of the ports and the station. The station's optimization problem is linked to the rest of the equations of the present work through (27) that shows the power drawn from the charging post by an EV is equal to the product of the battery's terminal voltage and charging current. Lastly, (28) finds the maximum power

absorbed by the station that is used to measure the demand charge.

The full model is presented in the next section.

F. Proposed Optimization Problem

Hitherto, the DC fast charging station is modeled, and the main constraints of the battery fast charging are formulated. In the following, the full model is presented.

$$\min \quad \alpha \int_t I(\tau)d\tau + (1-\alpha)\cdot(SOH(t_0) - SOH(t_f)) + \sum_n \sum_t P(n,t)(\lambda_b - \lambda_s) + P_d^{\max}\lambda_d, \tag{29}$$

subject to

$$(1)-(4),(13),(15),(22),(24)-(28),$$
$$z_{\min} \le z(t) \le z_{\max}, \tag{30}$$
$$z(t_0) = z_0, \tag{31}$$
$$z(t_f) = z_f, \tag{32}$$
$$SOH_{\min} \le SOH(t) \le SOH_{\max}, \tag{33}$$
$$SOH(t_0) = SOH_0, \tag{34}$$
$$I_{\min} \le I(t) \le I_{\max}, \tag{35}$$
$$V_{t,\min} \le V(t) \le V_{t,\max}, \tag{36}$$
$$T_{c,\min} \le T_c(t) \le T_{c,\max}, \tag{37}$$
$$T_c(t_0) = T_{c,0}, \tag{38}$$
$$T_s(t_0) = T_{s,0}, \tag{39}$$

where the initial, the minimum, and the maximum values of the optimization variables are set by (30)-(39). The objective function in (29) is composed of three parts. The first part enforces fast charging by increasing the current at the initial times and making it zero as soon as possible. The second part maximizes the health of the battery by mitigating the reduction of SOH. Finally, the last part is identical to (23).

The problem (29)–(39) is a nonlinear problem that, after discretization, can be solved through NLP solvers. In the next section, the numerical results are presented.

III. Numerical Results

In order to evaluate the effectiveness of the proposed approach, an illustrative example is presented in this section. The right-hand side of the state of health differential equation is replaced with a polynomial approximation for running the computer code. However, the main formula of ΔQ is used to calculate the actual capacity loss.

Table I shows the constant parameters used for the evaluation of the model. It is assumed that the batteries are charged from 20% to 80% of SOC and that the battery cells are fresh at the beginning, $SOH_0 = 1$. The temperatures are expressed in Kelvin. The environment temperature is assumed to be fixed at 25°C. Moreover, the core and surface temperatures of the cells are also 25°C at the beginning. The minimum and the maximum allowed core temperatures are 5°C and 45°C, respectively. The OCV of a cell is roughly 3.3 volts. Since there are 96 cells in parallel in the battery pack, the

TABLE I
Parameters of the Model

$SOH_0 = 1$	$SOH_{\max} = 1$	$SOH_{\min} = 0$	$T_f = 298$
$T_{c,0} = 298$	$T_{s,0} = 298$	$T_{c,\min} = 278$	$T_{c,\max} = 318$
$OCV = 317$	$V_{t,\min} = 192$	$V_{t,\max} = 345$	$I_{\min} = 0$
$I_{\max} = 1550$	$\gamma = 0.55$	$z_0 = 0.2$	$z_f = 0.8$
$R_1 = 0.026$	$R_2 = 0.026$	$C_1 = 1541$	$C_2 = 53958$
$R_0 = 0.013$	$C_s = 4.5$	$C_c = 62.7$	$R_c = 1.94$
$R_u = 3.19$	$C_b = 559440$	$R = 8.3$	$\lambda_b = 0.07$
$\lambda_d = 7.5$	$\lambda_s = 0.3$	$P^{\max}_{\text{charger}} = 250K$	

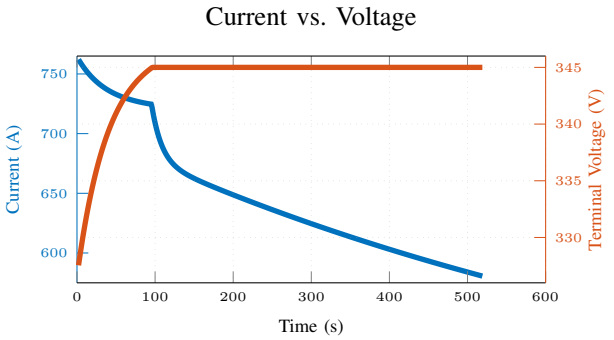

Fig. 4. Current and voltage evolution

pack's OCV is $96 \times 3.3 \approx 317$ (V). The same argument holds for the minimum and the maximum voltage terminals. For a cell, $V_{t,\min}$ and $V_{t,\max}$ are 2 and 4.2 volt, respectively. The maximum current is set equal to 10 times of the pack's C-rate, i.e., 155 Ah. Having 74 parallel 2.1 Ah cells in each module increases the pack's capacity to $74 \times 2.1 = 155.4$ Ah. Therefore, the pack's C-rate is 155 Ah. Moreover, in order to express the capacity in ampere seconds, it is multiplied by 3600, which yields $155.4 \times 3600 = 559440$ As. On the other hand, the energy and demand charge rates are \$0.07/kWh and \$7.5/kW, respectively. Lastly, the station sells electricity to the customers at the flat rate of \$0.3/kWh.

The results of optimized charging of one vehicle in the station are depicted in this case study. Fig. 4 illustrates the voltage and the current evolutions during the charging process. The current begins at 762.14 amperes and at 97 seconds reaches 718.67 amperes, beyond which its drop is expedited to maintain the voltage level unchanged. Ultimately, the current reaches 580.64 amperes at 520 seconds. Afterward, it becomes zero. The voltage, on the other hand, increases from 327.54 to 345 volt in the first 97 seconds. The 345 volt is the imposed maximum terminal voltage. The voltage remains the same until the battery reaches 80% of SOC. It is worth noting that based on Table 1 in [22], the voltage of DC stations could be between 50 and 700 volts, the current is between 100 and 1250 ampere, and the power rating ranges from 50 to 300kW.

The shape of the current curve is similar to two constant voltage (CV) charging steps. It starts from 4.9C (762.14 A) and monotonically decreases over 520s. The last value of the current is 3.74C (580.64 A), after which the current

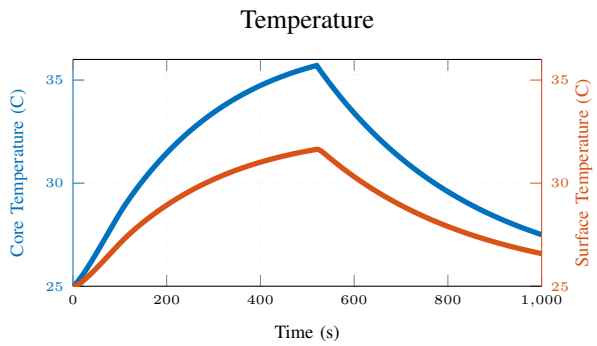

Fig. 5. Core and surface temperature alterations

immediately drops to zero. It takes $520/60 = 8.66$ minutes to increase the SOC from 20% to 80%. Note that the maximum C-rate limit is set to 10C. However, the power rating of the station's charger, $P_{\text{charger}}^{\max} = 250kW$, limits the product of current and voltage.

The changes in the battery's core and surface temperatures are depicted in Fig. 5. They keep increasing until $t = 521$ when the current drops to zero. Then they start to decrease. The rate of temperatures' elevation is negative due to the monotonic reduction of the current. As expected, the increase of core temperature is higher. In addition, core temperature is cooling faster because, according to (13) the cooling rate of core temperature depends on the difference between core and surface temperatures. In contrast, the rate of surface temperature cooling is affected by both core and ambient temperatures. The apex of core temperature is 35.68°C which is below $T_{c,\max} = 45$°C.

With one cycle of charging, the state of health (SOH) is reduced from 100% to 99.9964%, which is in an acceptable range.

IV. Conclusion

In this paper, the problem of electric vehicle fast charging is formulated in coordination with the DC fast charging station problem. The DCFC station enforces limitations on the battery's fast charging, which are properly considered through constraints. The EV battery is viewed as a battery pack consisting of 7104 lithium-ion cells. The mathematical model of the battery pack is built upon the cell's electro-thermal model. Moreover, an empirical aging model is adopted to take into account the battery's degradation due to fast charging. In the end, the model is assessed in a case study. The results demonstrate that, with infinitesimal deterioration of SOH, the proposed charging approach successfully increases the battery's SOC from 20% to 80% in less than nine minutes, while the battery temperature is kept under 40°C.

References

[1] W. Xie, X. Liu, R. He, Y. Li, X. Gao, X. Li, Z. Peng, S. Feng, X. Feng, and S. Yang, "Challenges and opportunities toward fast-charging of lithium-ion batteries," *Journal of Energy Storage*, vol. 32, p. 101837, 2020.

[2] Q. Ouyang, R. Ma, Z. Wu, and Z. Wang, "Optimal fast charging control for lithium-ion batteries," *IFAC-PapersOnLine*, vol. 53, no. 2, pp. 12435–12439, 2020.

[3] M. Abdel-Monem, K. Trad, N. Omar, O. Hegazy, P. Van den Bossche, and J. Van Mierlo, "Influence analysis of static and dynamic fast-charging current profiles on ageing performance of commercial lithium-ion batteries," *Energy*, vol. 120, pp. 179–191, 2017.

[4] P. M. Attia, A. Grover, N. Jin, K. A. Severson, T. M. Markov, Y.-H. Liao, M. H. Chen, B. Cheong, N. Perkins, Z. Yang, *et al.*, "Closed-loop optimization of fast-charging protocols for batteries with machine learning," *Nature*, vol. 578, no. 7795, pp. 397–402, 2020.

[5] Y. Gao, X. Zhang, Q. Cheng, B. Guo, and J. Yang, "Classification and review of the charging strategies for commercial lithium-ion batteries," *IEEE Access*, vol. 7, pp. 43511–43524, 2019.

[6] H. Perez, S. Dey, X. Hu, and S. Moura, "Optimal charging of li-ion batteries via a single particle model with electrolyte and thermal dynamics," *Journal of The Electrochemical Society*, vol. 164, no. 7, p. A1679, 2017.

[7] Z. Wei, C. Zou, F. Leng, B. H. Soong, and K.-J. Tseng, "Online model identification and state-of-charge estimate for lithium-ion battery with a recursive total least squares-based observer," *IEEE Transactions on Industrial Electronics*, vol. 65, no. 2, pp. 1336–1346, 2017.

[8] J. Liang, Y. Gan, W. Song, M. Tan, and Y. Li, "Thermal–electrochemical simulation of electrochemical characteristics and temperature difference for a battery module under two-stage fast charging," *Journal of Energy Storage*, vol. 29, p. 101307, 2020.

[9] T. Weaver, A. Allam, and S. Onori, "A novel lithium-ion battery pack modeling framework-series-connected case study," in *2020 American Control Conference (ACC)*, pp. 365–372, IEEE, 2020.

[10] T. R. Tanim, M. G. Shirk, R. L. Bewley, E. J. Dufek, and B. Y. Liaw, "Fast charge implications: Pack and cell analysis and comparison," *Journal of Power Sources*, vol. 381, pp. 56–65, 2018.

[11] J. Groot, *State-of-health estimation of li-ion batteries: Cycle life test methods*. Chalmers Tekniska Hogskola (Sweden), 2012.

[12] R. Buckreus, R. Aksu, M. Kisacikoglu, M. Yavuz, and B. Balasubramanian, "Optimization of multi-port dc fast charging stations operating with power cap policy," *IEEE Transactions on Transportation Electrification*, 2021.

[13] M. Li, M. Feng, D. Luo, and Z. Chen, "Fast charging li-ion batteries for a new era of electric vehicles," *Cell Reports Physical Science*, p. 100212, 2020.

[14] D. Erdemir and I. Dincer, "Assessment of renewable energy-driven and flywheel integrated fast-charging station for electric buses: A case study," *Journal of Energy Storage*, vol. 30, p. 101576, 2020.

[15] O. Elma, "A dynamic charging strategy with hybrid fast charging station for electric vehicles," *Energy*, vol. 202, p. 117680, 2020.

[16] S.-T. Ko, J. Lee, J.-H. Ahn, and B. K. Lee, "Innovative modeling approach for li-ion battery packs considering intrinsic cell unbalances and packaging elements," *Energies*, vol. 12, no. 3, p. 356, 2019.

[17] V. Azimi, A. Allam, W. T. Joe, Y. Choi, and S. Onori, "Fast charging-minimum degradation optimal control of series-connected battery modules with dc/dc bypass converters," in *2021 American Control Conference (ACC)*, pp. 231–236, IEEE, 2021.

[18] X. Lin, H. E. Perez, S. Mohan, J. B. Siegel, A. G. Stefanopoulou, Y. Ding, and M. P. Castanier, "A lumped-parameter electro-thermal model for cylindrical batteries," *Journal of Power Sources*, vol. 257, pp. 1–11, 2014.

[19] J. Wang, P. Liu, J. Hicks-Garner, E. Sherman, S. Soukiazian, M. Verbrugge, H. Tataria, J. Musser, and P. Finamore, "Cycle-life model for graphite-lifepo4 cells," *Journal of power sources*, vol. 196, no. 8, pp. 3942–3948, 2011.

[20] H. E. Perez, X. Hu, S. Dey, and S. J. Moura, "Optimal charging of li-ion batteries with coupled electro-thermal-aging dynamics," *IEEE Transactions on Vehicular Technology*, vol. 66, no. 9, pp. 7761–7770, 2017.

[21] A. Tomaszewska, Z. Chu, X. Feng, S. O'Kane, X. Liu, J. Chen, C. Ji, E. Endler, R. Li, L. Liu, *et al.*, "Lithium-ion battery fast charging: A review," *ETransportation*, vol. 1, p. 100011, 2019.

[22] T. D. Atmaja *et al.*, "Energy storage system using battery and ultracapacitor on mobile charging station for electric vehicle," *Energy Procedia*, vol. 68, pp. 429–437, 2015.